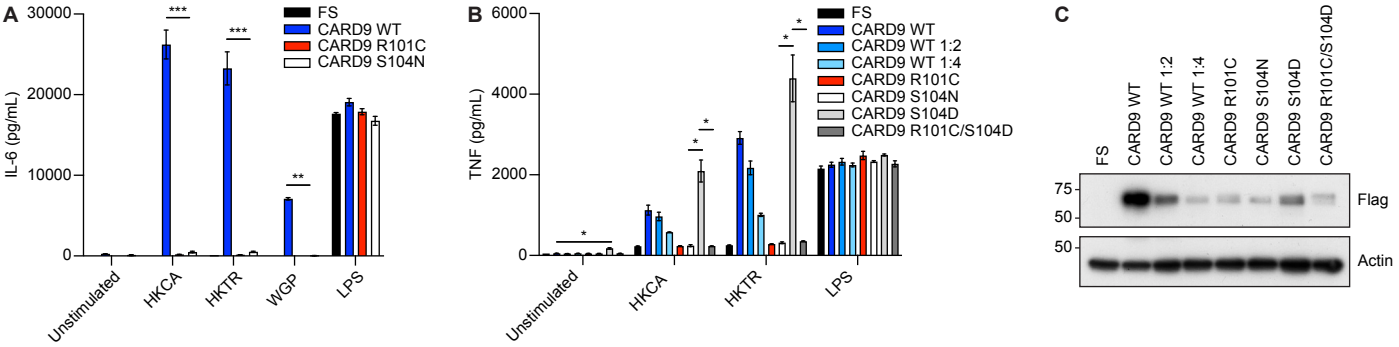

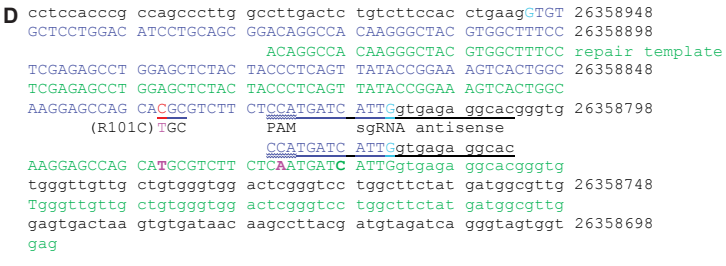

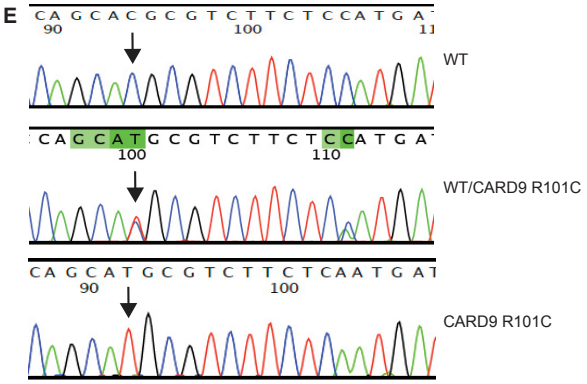

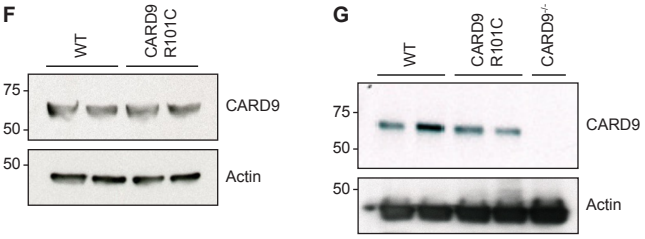

H

	pS104	R101C/pS104	S104
Clone	3702-2 BSA	LP01490 BSA	LP01491 BSA
4F9.A8	1.319	1.418	0.042
4F9.B7	1.517	1.572	0.045
4F9.C5	2.180	2.130	0.049
4F9.D3	2.700	2.447	0.058
4F9.F1	2.081	2.005	0.049
4F9.H5	2.376	2.278	0.054
15F3.B2	2.224	2.185	0.050
15F3.E8	2.473	2.215	0.050
15F3.F6	2.581	2.382	0.056
15F3.G4	2.451	2.439	0.054
15F3.H2	2.605	2.254	0.075
15F3.H4	2.617	2.422	0.083

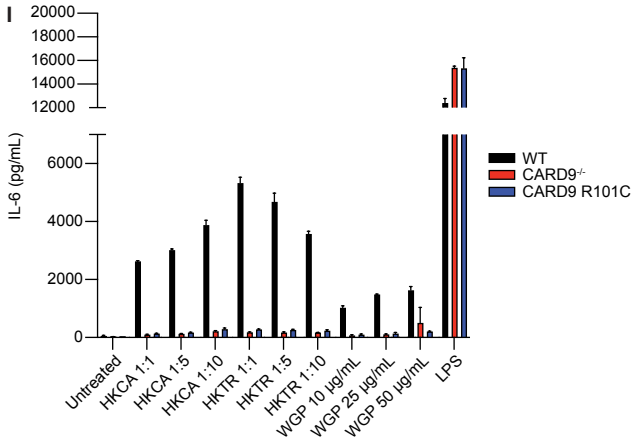

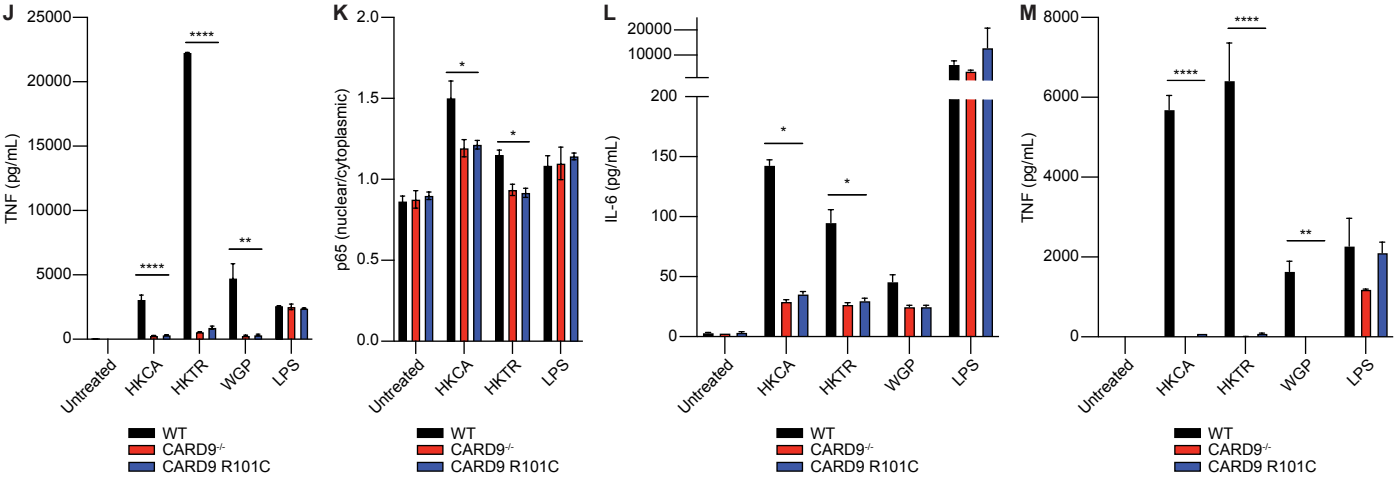

Figure S1. CARD9 linker residues R101 and S104 are required to elicit cytokine responses, Related to Figures 1 and 2.

(A) IL-6 concentration in the supernatants from *Card9*$^{-/-}$ BMDCs transduced with lentiviruses containing empty vector (FS), full-length CARD9 WT, CARD9 R101C, or CARD9 S104N and stimulated with HKCA (MOI 1:10), HKTR (MOI 1:10), WGP (50 μg/ml), or LPS (10ng/ml) for 24 h. (n=3 mice per condition).

(B) Tnf concentration in the supernatants from *Card9*$^{-/-}$ BMDMs transduced with lentiviruses containing empty vector (FS), CARD9 WT, CARD9 WT diluted 1:2, CARD9 WT diluted 1:4, CARD9 R101C, CARD9 S104N, CARD9 S104D, or CARD9 R101C/S104D and stimulated with HKCA (MOI 1:10), HKTR (MOI 1:10), or LPS (10 ng/ml) for 24 h. (n=3 mice per condition).

(C) Expression of CARD9 in the lysates from (B) determined by western blot with the indicated antibodies. Molecular weight markers (kDa) are shown to the left.

(D) Schematic representation of CRISPR knock-in of the *Card9* allele to obtain endogenous CARD9 R101C mutation.

(E) Sequencing result highlighting the presence of the mutated base pair (arrows).

(F-G) Representative western blots of (F) BMDCs and (G) splenic CD11c^{+} cells isolated from WT or Card9 R101C mice. Molecular weight markers (kDa) are shown to the left.

(H) Table summarizing hybridoma screening results for binding affinity of different pS104-specific antibodies. ELISA results are shown as values of absorbance at 490 nM, representing antibody reactivity towards pS104, R101C/pS104, or S104 peptides. The antibody used in the study is highlighted in yellow.

(I) IL-6 concentration in supernatants from WT, *Card9*$^{-/-}$, or Card9 R101C BMDCs treated with indicated concentrations of HKCA, HKTR, WGP, or LPS (10 ng/ml) for 24 h. (n=3 mice per condition).

(J) Tnf concentration in WT, *Card9*$^{-/-}$, or Card9 R101C BMDMs treated with HKCA (MOI 1:10), HKTR (MOI 1:10), WGP (50 μg/ml), or LPS (10 ng/ml) for 24 h.

(K) Nuclear p65 translocation in WT, *Card9*$^{-/-}$, or Card9 R101C BMDMs treated with HKCA (MOI 1:10), HKTR (MOI 1:10), or LPS (10 ng/ml) for 30 min.

(L) IL-6 concentration in supernatant from WT, *Card9*$^{-/-}$, or Card9 R101C bone marrow monocytes treated with HKCA (MOI 1:10), HKTR (MOI 1:10), WGP (50 μg/ml), or LPS (10 ng/ml) for 24 h.

(M) Tnf concentration in supernatant from WT, *Card9*$^{-/-}$, or CARD9 R101C bone marrow monocytes treated with HKCA (MOI 1:10), HKTR (MOI 1:10), WGP (50 μg/ml), or LPS (10 ng/ml) for 24 h.

Each experiment was repeated 3 times. Data represent mean +/- SEM. *p<0.05, **p<0.01, ***p<0.001, ****p<0.0001 from paired t-tests.

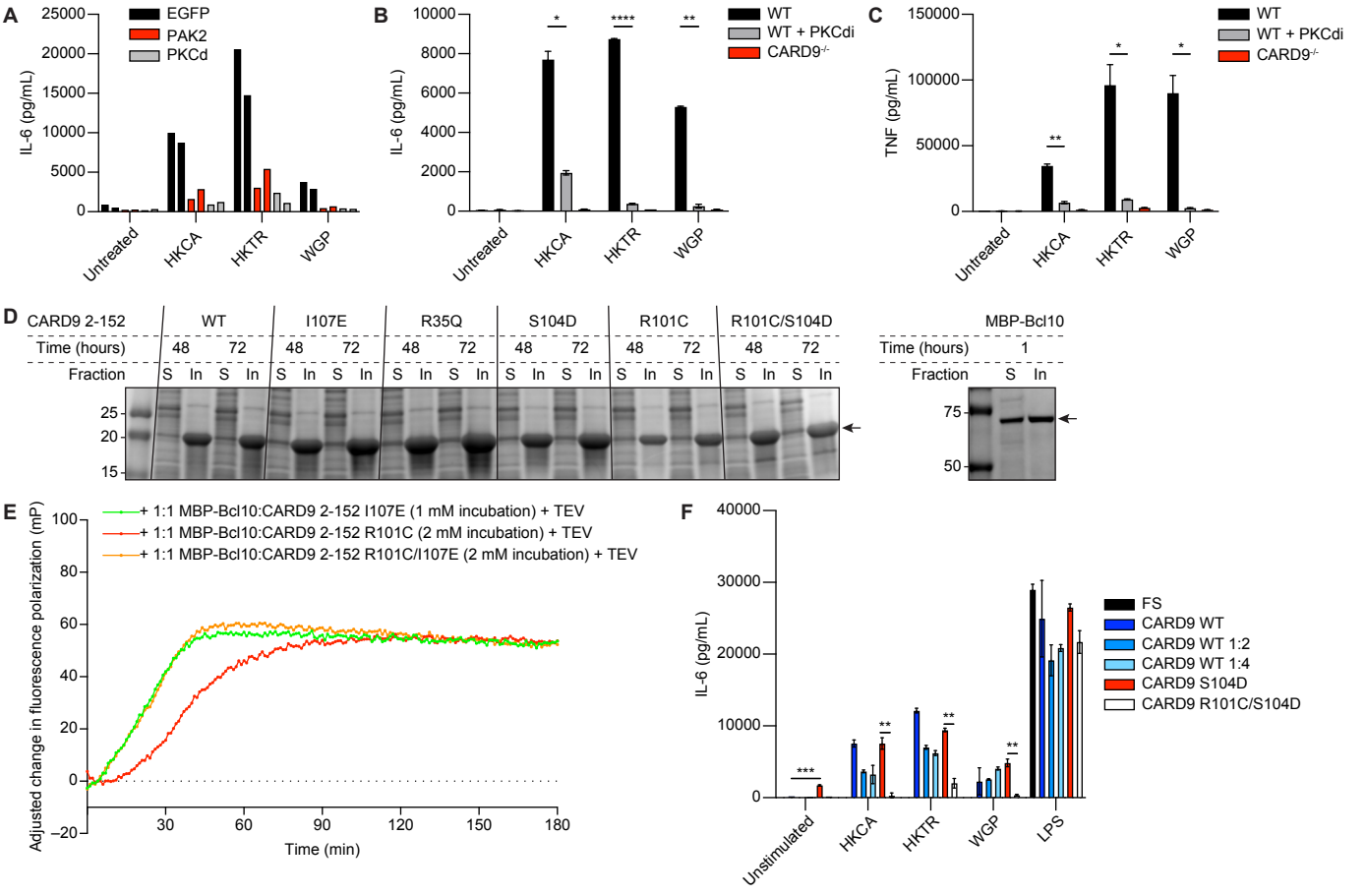

Figure S2. CARD9 R101 functions as a signaling switch activated by S104 phosphorylation, Related to Figure 3.

(A) IL-6 concentration in supernatant from BMDCs expressing Cas9 transduced with guides for the corresponding genes on day 2 and selected with puromycin. On day 9, cells were stimulated with HKCA (MOI 1:10), HKTR (1:10), or WGP (50 µg/ml) overnight.

(B) IL-6 concentration in supernatant from WT, WT pretreated with PKCdi (sotrastaurin), and *Card9*$^{-/-}$ BMDCs treated with HKCA (MOI 1:10), HKTR (MOI 1:10), or WGP (50 µg/ml) overnight.

(C) Tnf concentration in supernatant from WT, WT pretreated with PKCdi (sotrastaurin), and *Card9*$^{-/-}$ BMDCs treated with HKCA (MOI 1:10), or HKTR (MOI 1:10), or WGP (50 µg/ml) overnight.

(D) Representative western blot showing expression of CARD9 2-152 variants and MBP-BCL10 in BL21 DE3 cells at indicated timepoints from soluble (S) and insoluble (In) fractions. Molecular weight markers (kDa) are shown to the left.

(E) Normalized fluorescence polarization representing filament formation between different CARD9 2-152 variants and MBP-tagged BCL10 (average of quadruplicates).

(F) IL-6 concentration in supernatants from *Card9*$^{-/-}$ BMDCs transduced with lentiviruses containing empty vector (FS), CARD9 WT, CARD9 WT diluted 1:2, CARD9 WT diluted 1:4, CARD9 S104D, or CARD9 R101C/S104D and stimulated with HKCA (MOI 1:10), HKTR (MOI 1:10), WGP (50 µg/ml), or LPS (10 ng/ml) for 24 h. (n=3 mice per condition).

Each experiment was repeated 3 times. Data represent mean +/- SEM. *p<0.05, **p<0.01, ***p<0.001, ****p<0.0001 from paired t-tests.

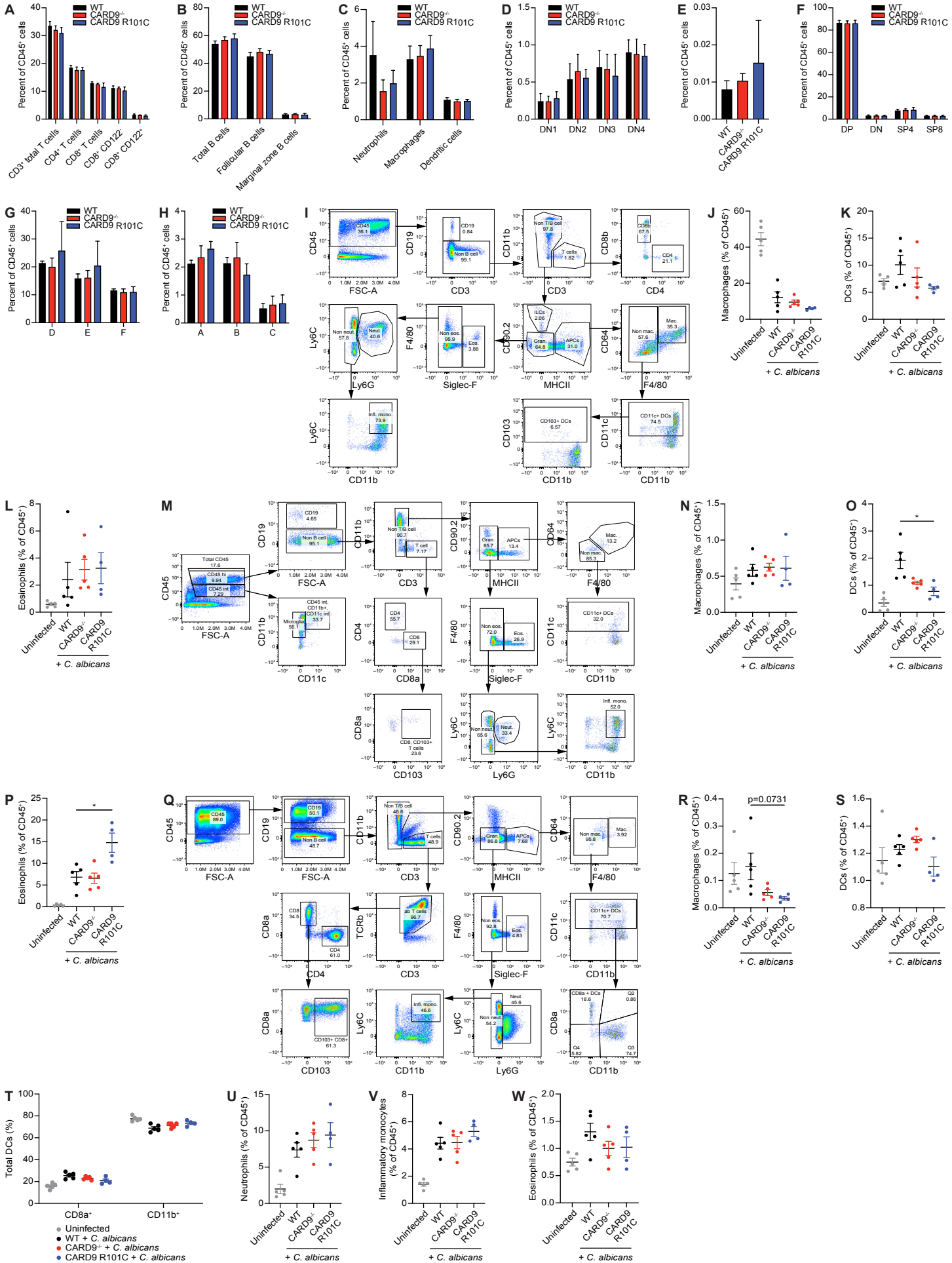
A
B
C
D
E
F
G
H
I
J
K
L
M
N
O
P
Q
R
S
T
U
V
W
WT
CARD9-/-
CARD9 R101C
Percent of CD45+ cells
CD3+ total T cells
CD4+ T cells
CD8+ T cells
CD8+ CD122+
CD8+ CD122+
Total B cells
Follicular B cells
Marginal zone B cells
Neutrophils
Macrophages
Dendritic cells
DN1
DN2
DN3
DN4
WT
CARD9-/-
CARD9 R101C
DP
DN
SP4
SP8
D
E
F
A
B
C
CD45
FSC-A
CD19
CD3
CD11b
CD8b
CD4
Ly6C
Ly6G
F4/80
Siglec-F
CD90.2
MHCII
CD64
CD103
CD11c
Macrophages (% of CD45+)
DCs (% of CD45+)
Uninfected
WT
CARD9-/-
CARD9 R101C
+ C. albicans
Eosinophils (% of CD45+)
CD8a
CD8a+
CD11b+
Total DCs (%)
Neutrophils (% of CD45+)
Inflammatory monocytes (% of CD45+)
Eosinophils (% of CD45+)
p=0.0731
*
Uninfected
WT + C. albicans
CARD9-/- + C. albicans
CARD9 R101C + C. albicans

Figure S3. Card9 R101C mice are predisposed to systemic fungal infection, Related to Figure 4.
(A) Flow cytometry analysis of T cell composition in the spleen from 12-week-old mice (n=4 for each genotype).
(B) Flow cytometry analysis of B cell composition in the spleen from 12-week-old mice (n=4 for each genotype). Total B cells ($B220^+$), follicular B cells ($B220^+$, $CD23^{hi}$, $CD21/35^{int}$), marginal zone B cells ($B220^+$, $CD21/35^{hi}$, $CD23^{low}$).
(C) Flow cytometry analysis of myeloid cell composition in the spleen from 12-week-old mice (n=4 for each genotype).
(D) Flow cytometry analysis of naïve T cell composition in the thymus from 12-week-old mice (n=4 for each genotype). DN1 ($CD44^+$, $CD25^-$), DN2 ($CD44^+$, $CD25^+$), DN3 ($CD44^-$, $CD25^+$), DN4 ($CD44^-$, $CD25^-$).
(E) Flow cytometry analysis of early T cell progenitor ($CD44^+$, $CD25^-$, $cKit^+$) composition in the thymus from 12-week-old mice (n=4 for each genotype).
(F) Flow cytometry analysis of T cell composition in the thymus from 12-week-old mice (n=4 for each genotype). DP ($CD4^+$, $CD8^+$), DN ($CD4^-$, $CD8^-$), SP4 ($CD4^+$, $CD8^-$), SP8 ($CD4^-$, $CD8^+$).
(G) Flow cytometry analysis of bone marrow Hardy fractions D-F from 12-week-old mice (n=4 for each genotype). Fractions D ($B220^+$, $CD43^-$), E ($B220^+$, $CD43^-$, IgM^+), F ($B220^+$, $CD43^-$, IgM^+, IgD^+).
(H) Flow cytometry analysis of bone marrow Hardy fractions A-C from 12-week-old mice (n=4 for each genotype). Fractions A ($B220^+$, $CD43^+$, $BP\text{-}1^-$, $CD24^-$), B ($B220^+$, $CD43^-$, $CD24^+$, $BP\text{-}1^-$), C ($CD22^+$, $CD43^+$, $CD24^+$, $BP\text{-}1^+$).
(I) Gating strategy applied to analyze kidney samples.
(J-L) Flow cytometry analysis of (J) macrophages, (K) dendritic cells (DCs), and (L) eosinophils in kidneys from mice injected intravenously with live *C. albicans* analyzed on day 2 post-injection (n=4 for each genotype).
(M) Gating strategy applied to analyze brain samples.
(N-P) Flow cytometry analysis of (N) macrophages, (O) DCs, and (P) eosinophils in the brains from mice injected intravenously with live *C. albicans* analyzed on day 2 post-injection (n=4 for each genotype).
(Q) Gating strategy applied to analyze spleen samples.
(R-W) Flow cytometry analysis of (R) macrophages, (S) total DCs, (T) $CD8a^+$ or $CD11b^+$ DCs, (U) neutrophils, (V) inflammatory monocytes, and (W) eosinophils in the spleens from mice injected intravenously with live *C. albicans* analyzed on day 2 post-injection (n=4 for each genotype).
Experiments were repeated at least 2 times. Data represent mean +/- SEM. *$p<0.05$ from paired t-tests.

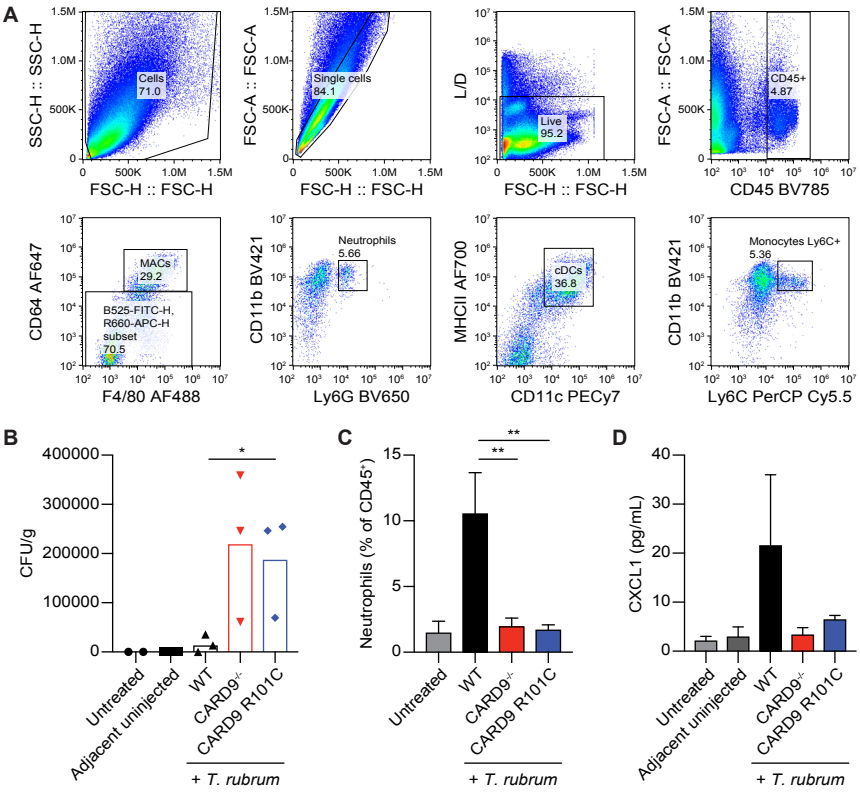

Figure S4. Card9 R101C mutation impairs spore clearance in a mouse model of dermatophytosis, Related to Figure 5.

(A) Gating strategy applied to skin samples.

(B) CFUs from foot pads of mice injected with live *T. rubrum* analyzed on day 9 post-injection (n=4 for each genotype).

(C) Flow cytometry analysis of neutrophils in the foot pads from mice in (B).

(D) Cxcl1 concentration in the foot pads from mice in (B) measured by ELISA.

Each experiment was repeated at least 2 times. Data represent mean +/- SEM. *p<0.05, **p<0.01 from paired t-tests.

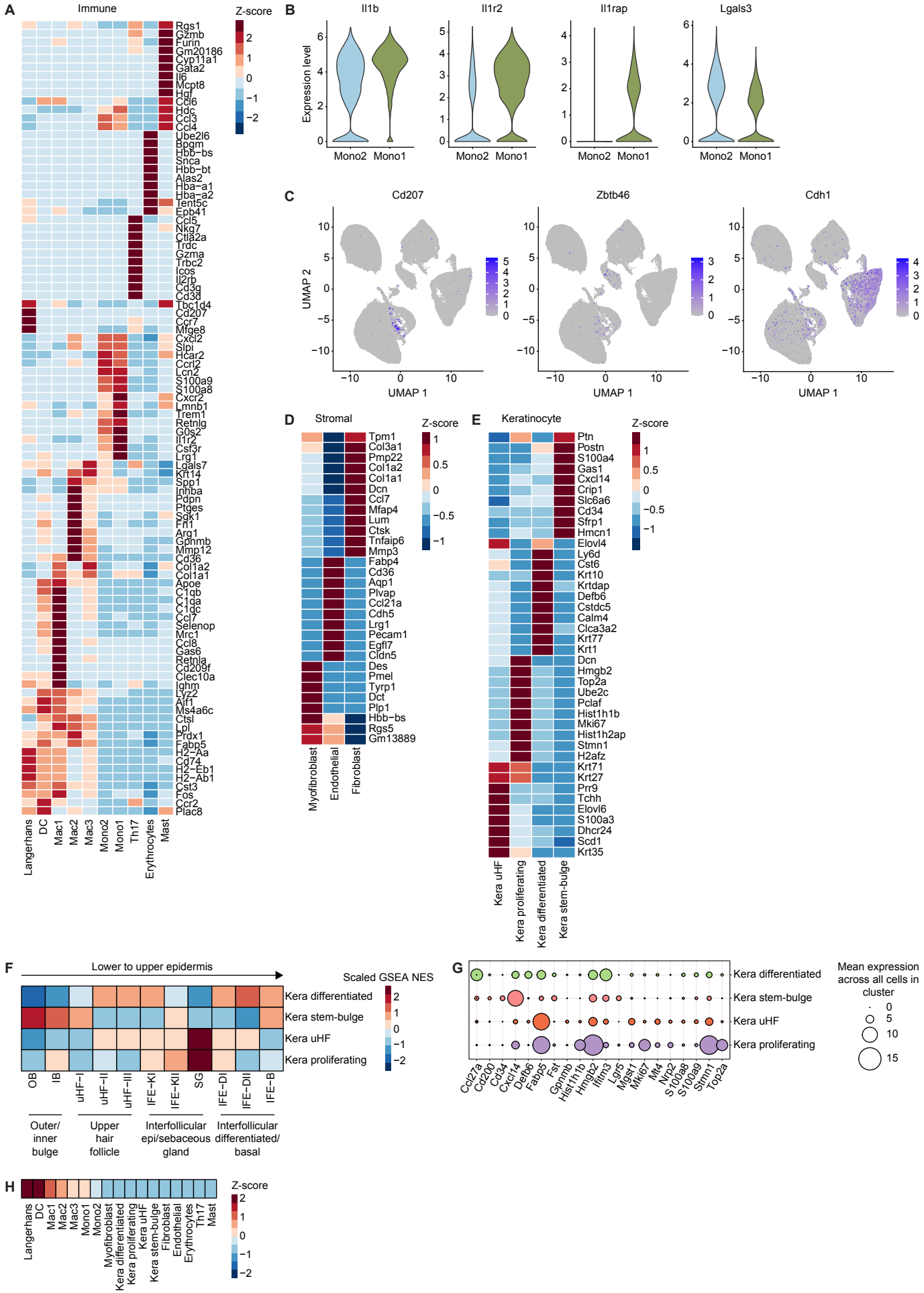
A
Immune
Z-score
Rgs1
Gzmb
Furin
Gm20186
Cyp11a1
Gata2
Il6
Mcpt8
Hgf
Ccl6
Hdc
Ccl3
Ccl4
Ube2l6
Bpgm
Hbb−bs
Snca
Hbb−bt
Alas2
Hba−a1
Hba−a2
Tent5c
Epb41
Ccl5
Nkg7
Ctla2a
Trdc
Gzma
Trbc2
Icos
Il2rb
Cd3g
Cd3d
Tbc1d4
Cd207
Ccr7
Mfge8
Cxcl2
Slpi
Hcar2
Ccrl2
Lcn2
S100a9
S100a8
Cxcr2
Lmnb1
Trem1
Retnlg
G0s2
Il1r2
Csf3r
Lrg1
Lgals7
Krt14
Spp1
Inhba
Pdpn
Ptges
Sgk1
Fn1
Arg1
Gpnmb
Mmp12
Cd36
Col1a2
Col1a1
Apoe
C1qb
C1qa
C1qc
Ccl7
Selenop
Mrc1
Ccl8
Gas6
Retnla
Cd209f
Clec10a
Ighm
Lyz2
Aif1
Ms4a6c
Ctsl
Lpl
Prdx1
Fabp5
H2−Aa
Cd74
H2−Eb1
H2−Ab1
Cst3
Fos
Ccr2
Plac8
Langerhans
DC
Mac1
Mac2
Mac3
Mono2
Mono1
Th17
Erythrocytes
Mast
B
Il1b
Il1r2
Il1rap
Lgals3
Expression level
Mono2
Mono1
C
Cd207
Zbtb46
Cdh1
UMAP 2
UMAP 1
D
Stromal
Z-score
Tpm1
Col3a1
Pmp22
Col1a2
Col1a1
Dcn
Ccl7
Mfap4
Lum
Ctsk
Tnfaip6
Mmp3
Fabp4
Cd36
Aqp1
Plvap
Ccl21a
Cdh5
Lrg1
Pecam1
Egfl7
Cldn5
Des
Pmel
Tyrp1
Dct
Plp1
Hbb−bs
Rgs5
Gm13889
Myofibroblast
Endothelial
Fibroblast
E
Keratinocyte
Z-score
Ptn
Postn
S100a4
Gas1
Cxcl14
Crip1
Slc6a6
Cd34
Sfrp1
Hmcn1
Elovl4
Ly6d
Cst6
Krt10
Krtdap
Defb6
Cstdc5
Calm4
Clca3a2
Krt77
Krt1
Dcn
Hmgb2
Top2a
Ube2c
Pclaf
Hist1h1b
Mki67
Hist1h2ap
Stmn1
H2afz
Krt71
Krt27
Prr9
Tchh
Elovl6
S100a3
Dhcr24
Scd1
Krt35
Kera uHF
Kera proliferating
Kera differentiated
Kera stem-bulge
F
Lower to upper epidermis
Scaled GSEA NES
Kera differentiated
Kera stem-bulge
Kera uHF
Kera proliferating
OB
IB
uHF−I
uHF−II
uHF−III
IFE−KI
IFE−KII
SG
IFE−DI
IFE−DII
IFE−B
Outer/ inner bulge
Upper hair follicle
Interfollicular epi/sebaceous gland
Interfollicular differentiated/ basal
G
Kera differentiated
Kera stem-bulge
Kera uHF
Kera proliferating
Ccl27a
Cd200
Cd34
Cxcl14
Defb6
Fabp5
Fst
Gpnmb
Hist1h1b
Hmgb2
Ifitm3
Lgr5
Mgst1
Mki67
Mt4
Nrp2
S100a8
S100a9
Stmn1
Top2a
Mean expression across all cells in cluster
H
Z-score
Langerhans
DC
Mac1
Mac2
Mac3
Mono1
Mono2
Myofibroblast
Kera differentiated
Kera proliferating
Kera uHF
Kera stem-bulge
Fibroblast
Endothelial
Erythrocytes
Th17
Mast

Figure S5. Top differentially expressed genes for immune, stromal, and keratinocyte clusters identified in scRNA-seq analysis, and additional markers expressed in keratinocytes, Related to Figure 6.

(A) Top 10 DEGs for each immune cluster. For each cluster, DEGs were defined as genes significantly differentially expressed (FDR $P < 0.05$) for the indicated cluster versus all other immune clusters.

(B) Log-normalized expression of representative markers differentiating the Mono1 and Mono2 clusters.

(C) Log-normalized expression of key markers defining Langerhans cells.

(D) Top 10 DEGs for each stromal cluster. For each cluster, DEGs were defined as genes significantly differentially expressed (FDR $P < 0.05$) for the indicated cluster versus all other stromal clusters.

(E) Top 10 DEGs for each keratinocyte cluster. For each cluster, DEGs were defined as genes significantly differentially expressed (FDR $P < 0.05$) for the indicated cluster versus all other keratinocyte clusters.

(F) GSEA showing that the keratinocyte clusters identified in the present study are enriched in previously identified keratinocyte states [S1]. Specifically, for each of our clusters, we used the full list of DEGs for the cluster as defined in (E) as input to a GSEA pre-ranked analysis using gene signatures for previously defined keratinocyte clusters [S1], indicated by the text labels beneath the heatmap. A high normalized enrichment score (NES) indicates positive enrichment of our clusters in the previously identified clusters [S1]; a low NES indicates negative enrichment of our clusters in the previously identified clusters [S1].

(G) Selected top DEGs for each of the four keratinocyte clusters. Dot size indicates mean expression across all cells in each cluster across timepoints and *Card9* genotypes.

(H) Relative expression of *Card9* across all immune clusters.

See also Tables S1-S4.

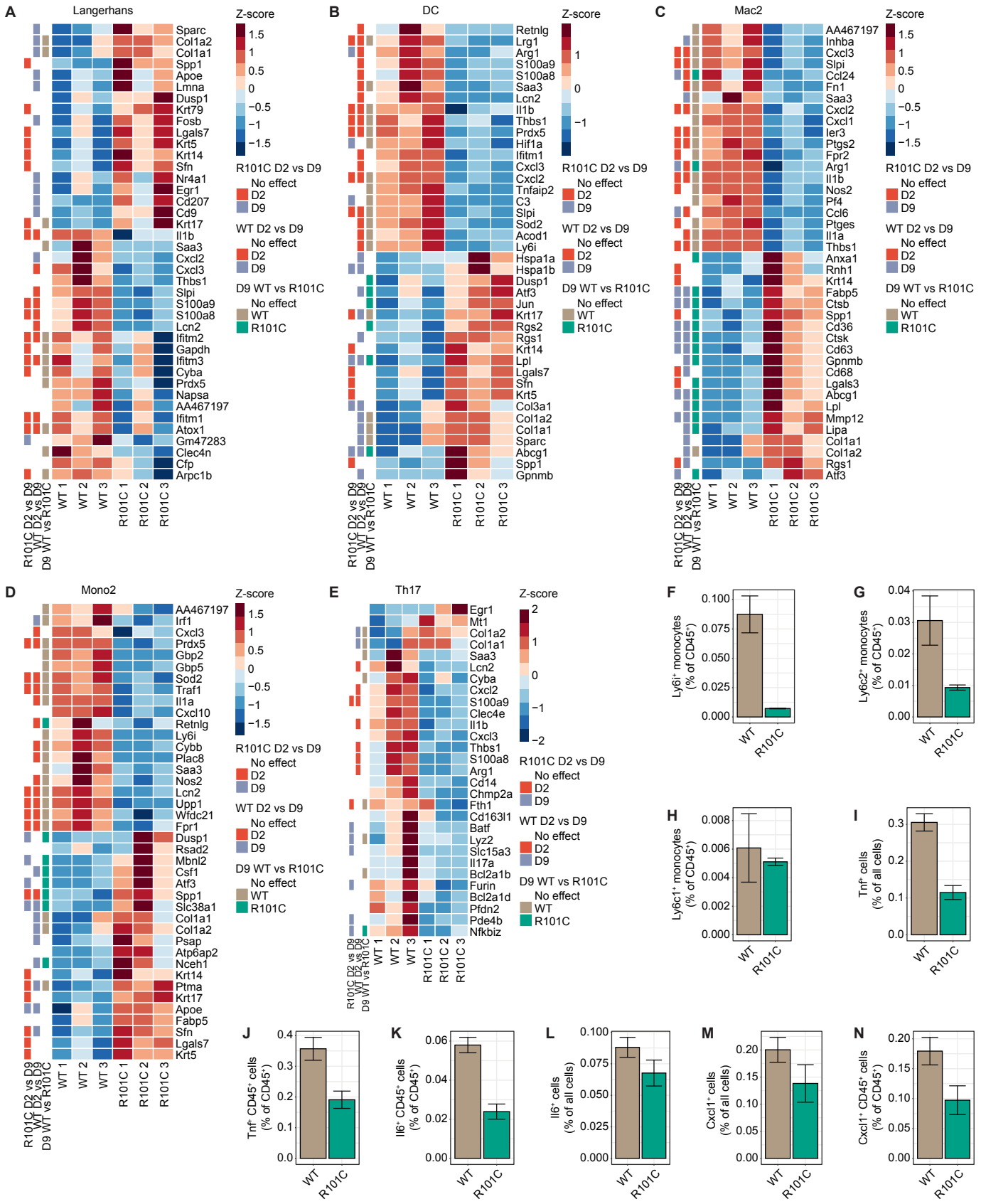

Figure S6. Top differentially expressed genes between WT and R101C cells for major immune clusters, Related to Figure 6.
(A-E) Heatmaps show top upregulated and downregulated genes for each cluster between WT and R101C cells at D2. Row annotations show differential expression of the corresponding gene for the R101C D2 vs D9 comparison, WT D2 vs D9 comparison, and D9 WT vs R101C comparison.
(F-H) Expression of Ly6C genes among CD45$^+$ cells in infected WT or R101C skin.
(I-N) Expression of cytokines and chemokines among CD45$^+$ cells in infected WT or R101C skin.
See also Tables S1-S4.

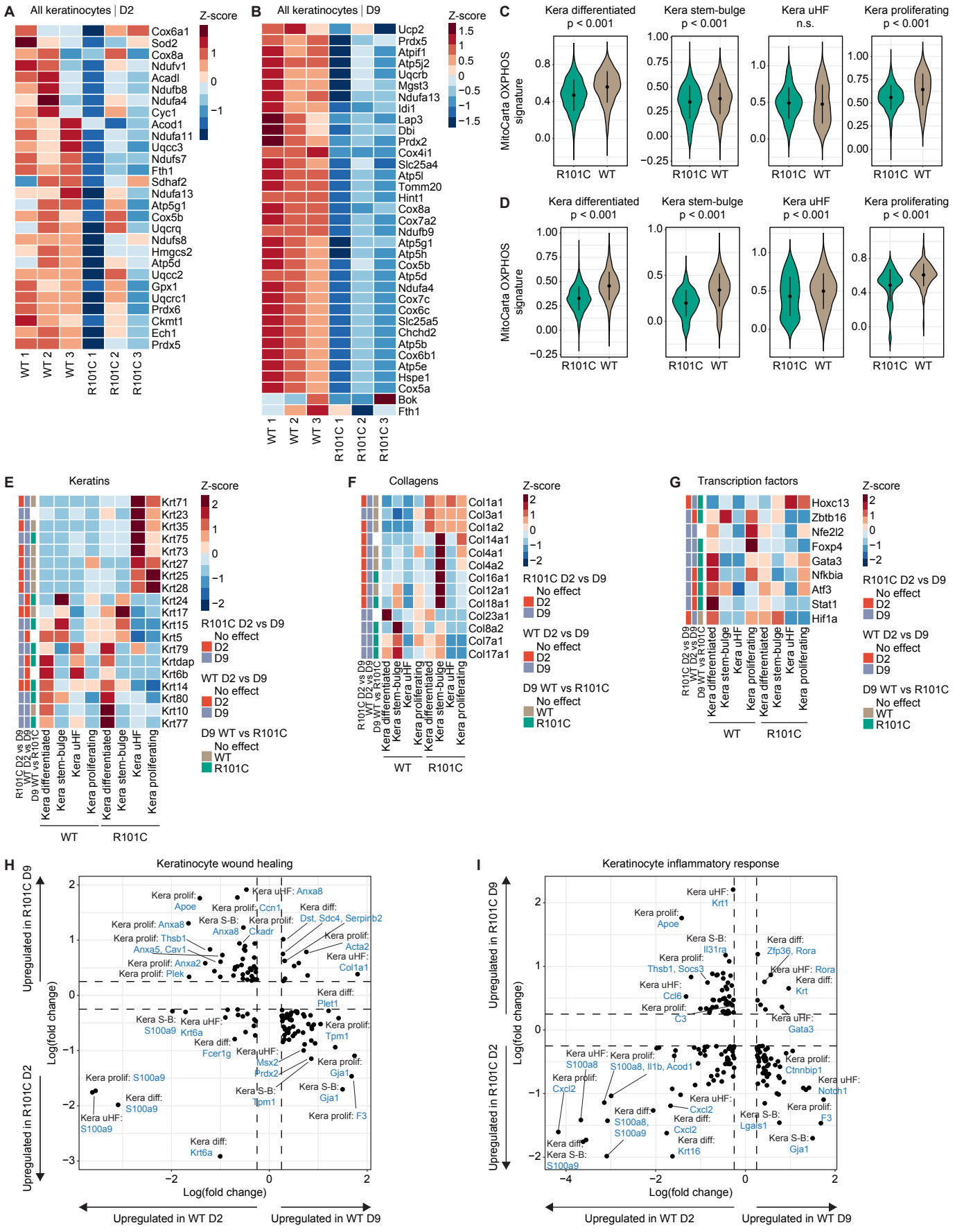

Figure S7. Additional gene families differentially expressed in keratinocytes, Related to Figure 7.

(A-B) Heatmap showing MitoCarta oxidative phosphorylation/stress genes differentially expressed in keratinocytes at (A) D2 and (B) D9.

(C-D) Application of the MitoCarta oxidative phosphorylation signature to (C) D2 and (D) D9 keratinocytes. P values

were calculated using a two-sided Wilcoxon test. n.s., not significant.
(E-G) Heatmaps showing (E) keratin family genes, (F) collagen family genes, and (G) transcription factors differentially expressed between WT and R101C keratinocytes.
(H) Wound healing genes from gene ontology differentially expressed in each keratinocyte cluster in WT and R101C cells at D2 or D9. Dotted lines indicate fold-change cutoff. Selected DEGs highlighted in blue.
(I) Inflammatory response genes from gene ontology differentially expressed in each keratinocyte cluster in WT and R101C cells at D2 or D9. Dotted lines indicate fold-change cutoff. Selected DEGs highlighted in blue.
See also Tables S3-S6.

Supplemental References

[S1] Joost, S., Zeisel, A., Jacob, T., Sun, X., La Manno, G., Lönnerberg, P., Linnarsson, S., and Kasper, M. (2016). Single-Cell Transcriptomics Reveals that Differentiation and Spatial Signatures Shape Epidermal and Hair Follicle Heterogeneity. Cell Syst 3, 221–237.e9.